RESEARCH ARTICLE

Central nervous system and peripheral cell labeling by vascular endothelial cadherin-driven lineage tracing in adult mice

Alejandro Soto-Avellaneda[1], Brad E. Morrison[1, 2, *]
1 Biomolecular Ph.D. Program, Boise State University, Boise, ID, USA
2 Department of Biological Sciences, Boise State University, Boise, ID, USA

Funding: *This study was supported by the National Institutes Health (grant Nos. 5P20GM109095 and P20GM103408) and Boise State University (to BEM).*

Abstract
Understanding the contribution of endothelial cells to the progenitor pools of adult tissues has the potential to inform therapies for human disease. To address whether endothelial cells transdifferentiate into non-vascular cell types, we performed cell lineage tracing analysis using transgenic mice engineered to express a fluorescent marker following activation by tamoxifen in vascular endothelial cadherin promoter-expressing cells (*VEcad-CreER^{T2}; B6 Cg-Gt(ROSA)26Sort$^{m9(CAG-tdTomato)Hze}$*). Activation of target-cell labeling following 1.5 months of *ad libitum* feeding with tamoxifen-laden chow in 4–5 month-old mice resulted in the tracing of central nervous system and peripheral cells that include: cerebellar granule neurons, ependymal cells, skeletal myocytes, pancreatic beta cells, pancreatic acinar cells, tubular cells in the renal cortex, duodenal crypt cells, ileal crypt cells, and hair follicle stem cells. As Nestin expression has been reported in a subset of endothelial cells, *Nes-CreER^{T2}* mice were also utilized in these conditions. The tracing of cells in adult *Nes-CreER^{T2}* mice revealed the labeling of canonical progeny cell types such as hippocampal and olfactory granule neurons as well as ependymal cells. Interestingly, Nestin tracing also labeled skeletal myocytes, ileal crypt cells, and sparsely marked cerebellar granule neurons. Our findings provide support for endothelial cells as active contributors to adult tissue progenitor pools. This information could be of particular significance for the intravenous delivery of therapeutics to downstream endothelial-derived cellular targets. The animal experiments were approved by the Boise State University Institute Animal Care and Use Committee (approval No. 006-AC15-018) on October 31, 2018.

***Correspondence to:**
Brad E. Morrison,
bradmorrison@boisestate.edu.

orcid:
0000-0002-6356-7149
(Brad E. Morrison)

doi: *10.4103/1673-5374.280317*

Received: *November 22, 2019*
Peer review started: *December 11, 2019*
Accepted: *January 3, 2020*
Published online: *April 3, 2020*

Key Words: *endothelial; lineage tracing; progenitor cells; transdifferentiation; ve-cadherin*

Chinese Library Classification No. *R446; R363; R741*

Introduction
Identifying cell populations in adult mammals that undergo regeneration and determining the source of progenitors can inform therapeutic strategies for a wide range of human diseases. For such strategies to succeed, consideration must be given to the contributions of non-canonical mechanisms for tissue regeneration. Supporting this notion is accumulating evidence indicating the existence of naturally occurring transdifferentiation mechanisms for adult cell replenishment (Michalopoulos et al., 2005; Tang et al., 2012; Tarlow et al., 2014; Merrell and Stanger, 2016). Endothelial cells are key players in human disease (Donato et al., 2015) while also representing an understudied potential pool of adult progenitor cells. These cells are particularly promising candidates due to the possibility of using intravenous genetic manipulation to target difficult to reach cell populations, such as those of the central nervous system, in conjunction with vectors currently employed in clinical trials (e.g., adeno-associated virus). Endothelial transdifferentiation would also offer an explanation for reported extravascular effects following intravenous delivery of viral vectors in humans and laboratory model systems. The proximity to all tissue types and a well-described association with adult progenitor cells (e.g., the perivascular stem cell niche) (Oh and Nör, 2015; Tamplin et al., 2015) provide additional rationale for further examination of endothelial cells in this context.

A growing body of evidence supports adult endothelial cell plasticity. For example, primary mouse neural progenitor cells have been observed to spontaneously differentiate into endothelial cells in culture (Wurmser et al., 2004). In addition, there is evidence that populations of adult neuronal progenitor cells migrate from the meninges, a region possessing a high concentration of endothelial cells (Bifari et al., 2017). Another area of attracting increased interest is the study of the endothelial-mesenchymal transition, which is a natural transdifferentiation phenomenon undertaken by endothelial cells and is an element of normal cardiac development (Bernanke and Markwald, 1982; Mjaatvedt et al., 1987; Eisenberg and Markwald, 1995; Camenisch et al., 2002; de Lange et al., 2004) that may also underlie several forms of vascular disease (Chen et al., 2015; Moonen et al., 2015; Li et al., 2018). Lastly, there is evidence that in adult rodents, specialized endothelial cells can de-differentiate to become smooth muscle cells and chondrogenic cells following vascular injury (Tang et al., 2012). These multipotent endothelial cells have been reported to readily differentiate into diverse cell types, including neurons *in vitro* (Tang et al., 2012). Tak-

en together, these findings blur the line between endothelial cells and other cell types, suggesting that endothelial cells could be attractive targets for cell lineage tracing analysis in an adult mammalian system.

The development of innovative cell lineage tracing approaches has accelerated research efforts in the field of regenerative medicine. Traditional cell lineage tracing methods that rely upon the labeling of replicated DNA (e.g., BrdU, [3H]-thymidine) would be expected to underreport transdifferentiation events due to the absence of cell division in this process. To address the limitations of traditional approaches, cell lineage tracing strategies that utilize a permanent fluorescent reporter activated by temporally-controlled genetic alteration have become prevalent (Kretzschmar and Watt, 2012). Therefore, to carry out a comprehensive cell lineage tracing study of endothelial transdifferentiation, we employed such a strategy that utilized an adult transgenic mouse model for specific temporal labeling of endothelial cells. Mice were sacrificed at varied intervals following the labeling period and 23 tissue types were assessed for the presence (or absence) of a fluorescent marker to identify cellular progeny.

Materials and Methods

Animals

All mouse procedures and husbandry were approved by the Boise State University Institute Animal Care and Use Committee (approval No. 006-AC15-018) on October 31, 2018. Mice were maintained in the Boise State University rodent vivarium at 25°C with 12-hour light/dark cycles and provided food ad libitum. VEcad-CreERT2 transgenic mice were kindly gifted by University of California, Los Angeles, USA (Monvoisin et al., 2006). Nes-CreERT2 transgenic mice (stock# 016261) (Battiste et al., 2007) and B6 Cg-Gt(ROSA)26Sor$^{tm9(CAG\text{-}tdTomato)Hze}$ reporter mice (stock# 007909) (Madisen et al., 2010) were purchased from Jackson laboratory (Bar Harbor, ME, USA). Cell lineage tracing experiments were initiated by replacing standard rodent pellets with chow containing 400 mg tamoxifen citrate/kg chow (Cat# TD.130860; Envigo, Huntingdon, Cambridgeshire, UK) as described previously (Albright et al., 2016; Rahman et al., 2017). After 1.5 months of tamoxifen treatment, the chow was replaced with standard rodent pellets. Both female and male 4–5-month-old mice were used in this study and no sex-linked variation in lineage tracing was observed. Genotyping for transgenic mouse lines was performed as described previously (Monvoisin et al., 2006; Battiste et al., 2007; Madisen et al., 2010). At least two mice per cohort were examined for reporter expression.

Tissue preparation and cryosectioning

Study mice were anesthetized with isoflurane followed by transcardial perfusion with heparin (20 U/mL) in neutral phosphate buffer (PB) and then 4% paraformaldehyde (PFA) in PB. Tissue was harvested and placed in ice-cold 4%PFA/PB and stored for 24 hours at 4°C. Samples were then transferred to a 30% sucrose/PB solution for storage at 4°C for 72 hours. Tissue was then dried and frozen rapidly in optimal cutting temperature (OCT) media on a block of dry ice. Samples were then wrapped in aluminum foil, placed in freezer bags and stored at –80°C until sectioning. Tissues were equilibrated to –20°C and then sectioned using a cryostat (model CM1950; Leica, Buffalo Grove, IL, USA) at a thickness of 15 μm directly onto Superfrost Plus Gold microscope slides (Thermo Fisher, Waltham, MA, USA). Slides were dried in a dark drawer overnight. The next day, slides were processed for labeling or placed in a slide holder, sealed, and stored at –80°C.

Hoechst dye labeling

Slides were removed from –80°C storage and allowed to equilibrate to room temperature in a dark drawer. Slides were then washed with PB and labeled with a 1:20,000 dilution of Hoechst 33342 dye (Cat# H3570; Thermo Fisher) for 10 minutes at room temperature. One PB wash was performed and sections were then allowed to dry in a dark drawer for 30 minutes. Coverslips were then mounted using Everbrite mounting media (Cat# 23003; Biotium, Fremont, CA, USA). Slides were allowed to dry in a dark drawer for 24 hours and then stored in a slide box at 4°C until viewed.

Immunohistochemistry

Section-containing slides were removed from –80°C storage and dried for 1 hour in the dark at room temperature. Antigen retrieval was performed as previously described (Hussaini et al., 2013). Slides were washed with PB and then placed in a container with citrate solution (Cat# 14746S; Cell Signaling, Danvers, MA, USA) diluted in dH_2O that was preheated in a microwave (5 minutes at high power). The solution with slides was then heated in a microwave for an additional 7 minutes at high power. The heated container was then covered and placed in an ice bath for 1 hour. Slides were then washed three times with a Tris solution (50 mM Tris HCl, 150 mM NaCl, 0.05% Triton X100-not pH adjusted). A pH-adjusted Tris solution was used (TBST: 50 mM Tris HCl, 150 mM NaCl, 0.05% Triton X100- pH 7.2) as a final wash. The slides were then dried for 30 minutes and primary antibodies were then diluted in TBST supplemented with donkey serum to 4%. The primary antibodies used in this study are as follows: anti-mCherry (Cat# MBS448092; 1:100; Mybiosource, San Diego, CA, USA), anti-NeuN (Cat# 24307S; 1:100; Cell Signaling), anti-insulin (Cat# 3014S; 1:800; Cell Signaling), anti-glucagon (Cat# sc-514592, 1:100; Santa Cruz Biotechnology, Dallas, TX, USA), and anti-K15 (Cat# sc-47697; 1:100; Santa Cruz Biotechnology). Antibody solutions were incubated in a humidifying slide chamber at room temperature overnight. The next day, slides were washed with TBST and incubated with the appropriate secondary antibodies diluted in TBST with donkey serum to 4% for 2 hours at room temperature. The secondary antibodies used in this study are as follows: donkey anti-goat Alexa 594 (Cat# A32758; 1:500; Thermo Fisher), donkey anti-mouse Alexa 488 (Cat# A-21202; 1:500; Thermo Fisher) and donkey anti-rabbit Alexa 488 (Cat# A-21206; 1:500; Thermo Fisher).

Slides were washed with TBST and then incubated with a 1:20,000 dilution of Hoechst 33342 dye (Cat# H3570; Thermo Fisher) at room temperature for 10 minutes. A final wash in PB was performed and slides were then dried for 1h in a dark drawer. Once dry, the slides were mounted with coverslips using Everbrite mounting media (Cat# 23003; Biotium). The coverslips were allowed to dry for 24 hours in a dark drawer before imaging or storage at 4°C.

Imaging and assessment of tissue sections

Conventional fluorescence microscopy images were obtained using an EVOS M7000 Imaging System (Thermo Fisher). Hoechst images were viewed using a DAPI filter cube and tdTomato was assessed using an RFP filter cube in the EVOS system. Semi-quantitative assessment of tdTomato+ve cells was performed by comparing three or more comparable levels of a tissue section obtained from at least two mice per cohort. Cells were counted at 100× fields and a relative number of "+" signs assigned. When comparing across different cohorts within a tissue group, the number of + signs correlate to relative increases or decreases in tdTomato +ve cell number. As such, this method is not stereological but provides a strong correlation with the relative abundance of cells expressing tdTomato. Confocal microscopy images were acquired using the following systems: Zeiss Laser Scanning Confocal Microscope Meta 510 system (Zeiss, White Plains, NY, USA), Zeiss 880 Airy Scan system and an Olympus FV3000 Laser Scanning Confocal Microscope system (Olympus, Center Valley, PA, USA). A supplemental image database containing representative conventional fluorescence microscopy images (EVOS M7000 system) from all examined tissues can be found at the Open Science Framework (https://osf.io/x9yu8).

Results

VE-cadherin cell lineage tracing labels a diversity of cell types in adult mice

Endothelial cell labeling was performed using a double transgenic mouse system that allows for VE-cadherin promoter-specific expression of a CRE-recombinase (*VEcad-CreER^{T2}*) (Monvoisin et al., 2006), kindly provided by Dr. Iruela-Arispe (UCLA)) that is activated at designated times by the addition of tamoxifen (TAM) to rodent chow (**Figure 1**). Following activation by TAM, *CreER^{T2}* excises a loxP-flanked DNA cassette containing a stop codon within a transgenic CAG-promoter-driven tdTomato reporter (Gt(ROSA)26Sor$^{tm9(CAG-tdTomato)Hze}$) (Madisen et al., 2010), resulting in permanent and constitutive expression of tdTomato. VE-cadherin-directed *CreER^{T2}* expression was selected due to the high degree of endothelial cell specificity reported in adult mice (Heimark et al., 1990; Monvoisin et al., 2006). We also observed prototypical endothelial cell tracing in these mice (**Additional Figure 1**). For this study, we sought to extend the labeling period to 1.5 months to enhance the tagging of transient endothelial cell populations not covered by previous studies (**Figure 1B**). In addition, we lengthened the post-labeling phase (1.5, 3, and 6 months) for increased capture of slow transdifferentiation events. A summary of the results for the examined cell types and tissues is found in **Table 1**. In addition, a repository of images containing transgenic mouse lines, tissues, and experimental time points has been provided in **Additional file 1**.

Central nervous system

Examination of the central nervous system (CNS) following TAM treatment revealed tdTomato-positive cells in several cell types not previously reported to share embryonic origins with endothelial cells. Positive cellular projections were observed in the olfactory bulb adjacent to but outside of glomeruli, suggesting that these cells are not olfactory neurons (**Figure 2**). These projections were noted in a juxtaglomerular region within all levels of olfactory bulb sections and at all post-TAM treatment time points. No associated somas were observed, suggesting that these projections originated outside of the olfactory bulb.

Interestingly, numerous tdTomato$^+$ cells were detected in the granule layer of the cerebellum (**Figure 2**). Positive cellular projections within the molecular layer were detected and confocal microscopic examination (**Figure 3A**, **Additional Figures 2A** and **4**) confirmed that the abundant positive cells in this region were cerebellar granule neurons (CGNs). A clear gradation of positive CGN expression was observed, with a peak at 3 months post-TAM treatment and with complete absence observed at 6 months. The choroid plexus lining the ventricle ventral to the cerebellum was tdTomato$^+$ at all time points, with peak frequency of tdTomato expression occurring 3 months following TAM treatment. The subventricular zone (SVZ), a region possessing adult olfactory bulb neuronal progenitors, exhibited positive labeling only in the ependymal layer (SVZ layer I) at 3 months of age (**Figure 2**).

Hair follicle stem cells

Inspection of integumentary tissue obtained from the dorsal pelt of adult transgenic mice revealed tdTomato expression within hair root tissue (**Figure 4**). The most robust labeling was observed 1.5 months after TAM treatment, with labeling decreasing at 3 months and reaching undetectable levels at 6 months. Confocal microscopic assessment (**Figure 3B** and **C** and **Additional Figure 2B–D**) revealed that a small portion of tdTomato-expressing cells co-label with the hair root stem cell marker K15. It is interesting to note the numerous instances in which tdTomato-labeled cells were observed in close proximity to K15-expressing cells without exhibiting co-localization (**Additional Figure 2B–D**).

Skeletal muscle

The hamstrings of adult mice were also inspected for tdTomato labeling (**Figure 4** and **Additional Figure 3**). Surprisingly, extensive labeling was observed at 1.5 months, with maximum labeling observed 3 months after TAM treatment. After 6 months, faint fluorescence was still evident surrounding muscle fibers, indicating labeling within the endomysium region with possible satellite cell involvement.

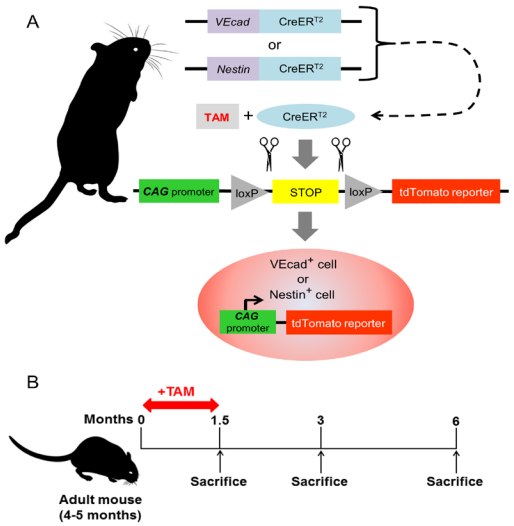

Figure 1 Transgenic mouse cell lineage tracing strategy.
(A) Adult mice (4–5 months of age) possessing a transgenic cassette containing either vascular endothelial cadherin (VEcad)- or Nestin-promoter-driven CreER^{T2} recombinase are fed tamoxifen (TAM) citrate-laden chow to activate loxP site-directed excision of a second transgene (Ai9 line) possessing a translation stop codon sequence. Removal of this stop codon results in CAG promoter-driven reporter expression of tdTomato. Note that post-TAM tdTomato expression is solely controlled by the CAG promoter and Gt(ROSA)26Sor chromosomal locus (tdTomato reporter locus). (B) Permanent activation of tdTomato expression in VEcad or Nestin-expressing cells was achieved by feeding adult mice tamoxifen for 1.5 months. Mice were sacrificed at the indicated times, fixed and histological assessment was performed.

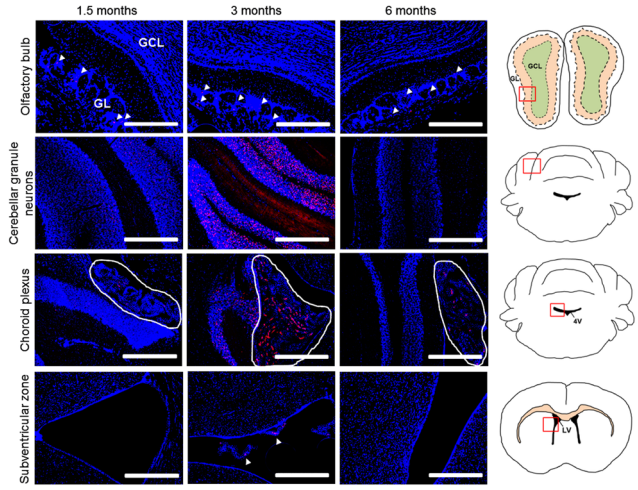

Figure 2 Vascular endothelial-cadherin cell fate mapping in the central nervous system.
Adult mice possessing *VEcad-CreER^{T2}/Rosa-flox-STOP-tdTomato* were fed tamoxifen-containing chow for 1.5 months and mice sacrificed at the indicated times following initiation of treatment. Representative channel merged images from fixed and Hoechst labeled tissues. Nuclei are labeled by Hoechst (blue) and cell lineage tracing is indicated by tdTomato (red). The areas shown in micrographs are indicated by highlighted regions (red boxes) in diagrams to the right where the granule cell layer (GCL), glomerular layer (GL), lateral ventricle (LV) and fourth ventricle (4V) are shown. Arrowheads highlight labeled cells and cellular appendages (white scale bars: 400 μm).

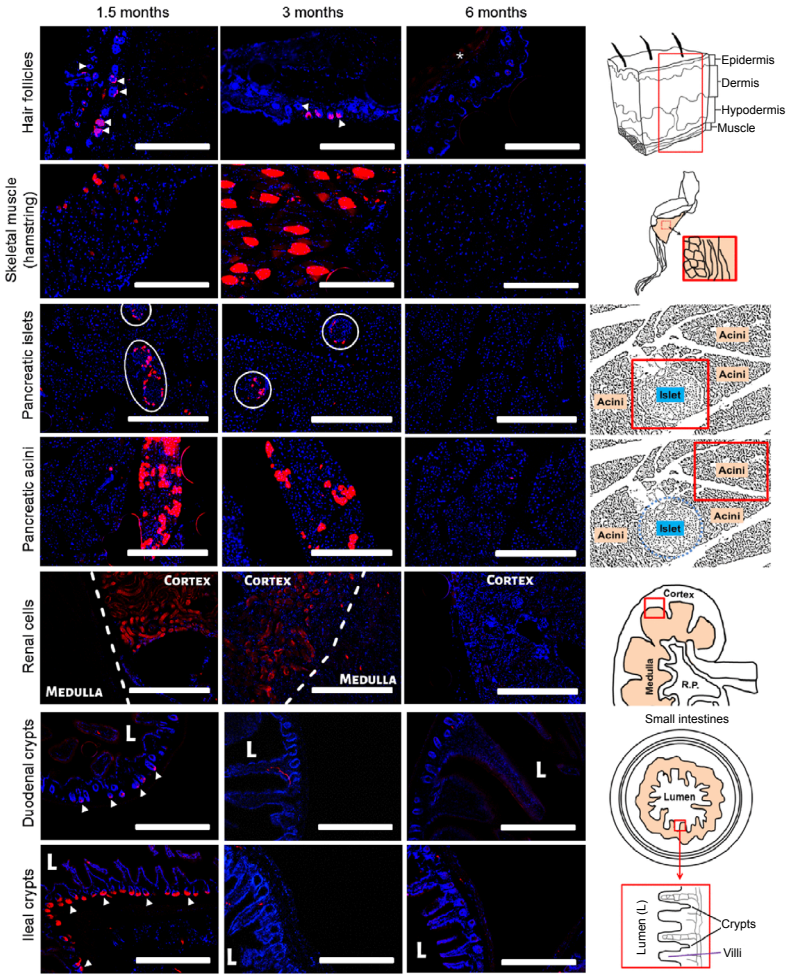

Figure 4 Vascular endothelial-cadherin cell fate mapping in the periphery.
4–5-Month-old *VEcad-CreER^{T2}/Rosa-flox-STOP-tdTomato* mice were provided tamoxifen chow for 1.5 months and sacrificed at the times shown. Images were obtained from fixed and Hoechst stained tissues. Cell lineage tracing is evidenced by tdTomato (red) and nuclei are indicated by Hoechst (blue) labeling. Arrowheads highlight labeled cells (white scale bar = 400 μm). Red boxes displayed in diagrams indicate region shown in the associated micrographs. Asterisk (*) indicates tdTomato$^+$ muscle fibers underlying skin; Intestinal lumen (L) and tdTomato$^+$ crypt cells (arrowheads) are labeled. Renal tissue diagram indicates the location of the renal pelvis (R.P.).

Table 1 Cell lineage tracing results for vascular endothelial cadherin and Nestin

Cell type	1.5 mon post-TAM	3 mon post-TAM	6 mon post-TAM
A. Vascular endothelial cadherin cell lineage tracing			
Olfactory bulb granule neurons	–	–	–
Olfactory bulb juxtaglomerular projections	++	++++	++
Midbrain neurons	–	–	–
Midbrain ventricular cells	–	–	–
Cortical neurons	–	–	–
Hippocampal neurons	–	–	–
Cerebellar granule neurons	++++	++++++	–
Choroid plexus	+++	+++++	+++
Striatal neurons	–	–	–
Subventricular zone layer I	–	++	–
Subventricular zone layers 2–4	–	–	–
Pancreatic islet cells	+++++++	++++	–
Pancreatic acinar cells	+++++++	++++	–
Skeletal myocytes (hamstring)	++	+++++	++[a]
Skeletal myocytes (underlying dorsal skin)	–	–	++++
Cardiac myocytes	–	–	–
Hepatocytes	–	–	–
Renal cells (cortical layer)	+++++	+++	–
Hair follicle cells	+++++	++	–
Splenic follicles	–	–	–
Gastric pit cells	–	–	–
Duodenal crypt cells	+++	–	–
Ileal crypt cells	++++++++++	–	–
Colonic crypt cells	–	–	–
B. Nestin cell lineage tracing			
Olfactory bulb granule neurons	–	+++++	+++++++
Olfactory bulb juxtaglomerular projections	+	++++	++
Midbrain neurons	–	–	–
Midbrain ventricular cells	–	+++++	++
Cortical neurons	–	–	–
Hippocampal neurons	–	+	++
Cerebellar granule neurons	–	++	+
Choroid plexus	++	–	+++
Striatal neurons	–	–	–
Subventricular zone layer I	–	++++++++	++++++
Subventricular zone layers 2–4	–	–	–
Pancreatic islet cells	–	–	–
Pancreatic acinar cells	–	–	+
Skeletal myocytes (hamstring)	–	+++	+
Skeletal myocytes (underlying dorsal skin)	–	+	+++
Cardiac myocytes	–	–	–
Hepatocytes	–	–	–
Renal cells	–	–	–
Hair follicle cells	–	–	–
Splenic follicles	–	–	–
Gastric pit cells	–	–	–
Duodenal crypt cells	–	–	–
Ileal crypt cells	++++++++[b]	–[c]	++[d]
Colonic crypt cells	–	–	–

Cell types were scored semi-quantitatively for the relative abundance of tdTomato positive cells (+) at the indicated times following initiation of tamoxifen treatment in (A) *VEcad-CreER^{T2}/Rosa-flox-STOP-tdTomato* or (B) *Nes-CreER^{T2}/Rosa-flox-STOP-tdTomato* transgenic mice. Cell types without (–) tdTomato labeling are also shown. Notes: [a]myocytes very weakly labeled with most signal surrounding the muscle fiber; [b]abundant weakly positive cells; [c]possible tdTomato$^+$ tumor noted; [d]weakly positive.

No strongly labeled muscle fibers were observed for that time point. Labeling was concentrated in localized regions of muscle whenever robust tdTomato expression was observed (1.5 and 3 months post-TAM), leaving most areas of muscle with no labeled fibers. In addition, muscle residing beneath the subcutaneous layer of dorsal skin was found to be weakly tdTomato$^+$ at 6 months post-TAM with no detectable fluorescence at 1.5 or 3 months (**Figure 4**).

Pancreas

Another unexpected finding was the observed labeling of pancreatic islets (**Figure 4**). There was a well-defined gradation of labeling, with all observed islets possessing tdTomato-positive cells 1.5 months post-TAM and with 83% of islets containing one or more positive cells 3 months post-TAM. No tdTomato$^+$ cells were observed 6 months post-TAM. Confocal microscopic analysis (**Figure 5A** and **Additional Figure 5A**) revealed that some of the positive cells were beta cells (3% insulin$^+$). It is worthwhile to note the extremely close proximity of the tdTomato-positive cells with insulin-positive cells in an interwoven configuration (**Figures 5A** and **B** and **Additional Figure 5A** and **B**). Co-labeling with glucagon (**Figure 5C** and **Additional Figure 5C**) was not observed, indicating that none of the tdTomato-expressing cells at these time points were alpha cells.

TdTomato labeling was also detected in the acini of the exocrine pancreas (**Figure 4** and **Additional Figure 6**). The most robust labeling was observed at 1.5 months and decreasing thereafter. Only a small minority of pancreatic acini exhibited positive labeling. Similar to the pattern witnessed in skeletal muscle, positive cells were most often grouped in close proximity to each other. Likewise, only a very faint fluorescent signal in acini was detected 6 months post-TAM.

Renal cells

Kidney sections were assessed and found to exhibit strong tdTomato expression 1.5 months after TAM administration (**Figure 4**). Labeling was restricted to the cortical layer and markedly absent from the medulla. This suggests that tdTomato labeling was likely confined to proximal and distal convoluted tubules. Expression intensity diminished significantly 3 months post-TAM and was only very weakly detectable

in the cortex at 6 months. It should be noted that residual urea would have been flushed from the tissue sections by numerous washes associated with sample preparation before imaging. Therefore, it is not expected that filtrate or urine (which might exhibit tdTomato fluorescence) contributed to the observed signal.

Small intestines

Examination of the intestinal tract revealed positive tdTomato labeling for crypt cells (crypt of Lieberkühn) found in both the duodenum and ileum (**Figure 4**). These labeled cells were concentrated within the most basal portion of the intestinal gland. The most intense labeling was observed 1.5 months post-TAM and labeling was completely absent (or very indistinct) 3 and 6 months following TAM treatment. No fluorescence was observed for colonic cells at any time point.

Nestin cell lineage tracing labels for canonical and non-canonical targets in adult mice

The intermediate filament Nestin is known to exhibit a promiscuous expression pattern. However, it has been reported that some endothelial cells (as well as specialized endothelial progenitor cells) express Nestin in adult mice (Mokrý et al., 2008; Suzuki et al., 2010; Ding and Morrison, 2013; Itkin et al., 2016; Dusart et al., 2018). Therefore, Nestin cell lineage tracing (*Nes-CreER*^{T2}), as employed here (**Figure 1**), could provide additional information with respect to endothelial cell progeny. We found both canonical Nestin cell progeny as well as novel cell labeling events show some correlation with VE-cadherin cell lineage tracing. A detailed summary of Nestin cell lineage tracing results can be found in **Table 1** and additional image sets are provided in **Additional file 1**.

Central nervous system

Analysis of adult mouse brain (**Figure 6**) showed tdTomato labeling of neurons in the granule cell layer of the olfactory bulb at 3 months, which was maintained at a similar level 6 months post-TAM. This is consistent with previous reports of Nestin-positive progenitors migrating from the SVZ to establish adult-born olfactory bulb neurons (Altman, 1969; Menezes et al., 1995; Zerlin et al., 1995). Labeled olfactory neurons were not present at 1.5 months, which indicates that the tdTomato-expressing cells at 3 months were indeed derived outside of the olfactory bulb. Interestingly, we observed juxtaglomerular projections in the olfactory bulb at all time points, as was witnessed in VE-cadherin lineage tracing experiments described above. No associated cell somas were noted, which indicates that these projections originated outside of the olfactory bulb. Similar to adult olfactory bulb granule neurons, populations of hippocampal cells are known to undergo adult neurogenesis from Nestin^{+} progenitors (Palmer et al., 1995). Supporting this notion, we find tdTomato-positive cells in the hippocampus beginning 3 months following TAM administration and increasing at 6 months. Interestingly, we find only a relatively small number of labeled cells in this region, despite numerous reports in the literature of abundant neuronal regeneration in the hippocampus of adult mice (Altman and Das, 1965; Bayer et al., 1982).

Our study also detected tdTomato-labeled cerebellar granule neurons at 3 and 6 months following treatment with TAM (**Figure 6**). No tdTomato-positive cells were noted in the 1.5-month cohort. Both the 3- and 6-month groups exhibited far fewer positive cerebellar granule neurons compared to our VE-cadherin study. Assessment of the nearby choroid plexus showed sparse labeling at 1.5 and 6 months. Surprisingly, no labeled cells were observed 3 months after TAM treatment for the cohort of mice we examined. This correlates inversely with VE-cadherin labeling of the same structure at 3 months. Another interesting finding was positive labeling of ependymal cells lining the ventricular surfaces extending throughout the brain, which was absent at 1.5 months but robustly labeled 3 and 6 months post-TAM. The expression pattern also shows a clear disconnect between the choroid plexus and the ubiquitous ependymal layer indicating differential regulation for their production.

Skeletal muscle

Investigation of skeletal muscle obtained from hamstring found tdTomato-labeled muscle fibers 3 months after TAM treatment while being absent in the 1.5-month group (**Figure 7**). However, the 6-month cohort showed positive labeling for very few muscle fibers. It is evident that the majority of positive cells at 3 months have an elevated signal originating from the endomysium area in addition to signals originating from myocytes. Comparable to VE-cadherin tracing, Nestin-traced myocytes were found in close proximity to each other. We also observed robust Nestin tracing to muscle underlying the subcutaneous fat layer of dorsal skin at 3 and 6 months post-TAM but not at 1.5 months (**Figure 7**).

Small intestine

Nestin cell lineage tracing revealed positive labeling for ileal crypt cells at 1.5 months and absence at 3 and 6 months post-TAM treatment (**Figure 7**). Labeling was analogous to VE-cadherin tracing for this tissue. Conversely, no labeling was observed for duodenal crypt cells, suggesting divergent mechanisms for these two tissues. Interestingly, a small mass of tdTomato-positive cells possessing irregular morphology (possible tumor) was noted in the ileum of a 3 month post-TAM mouse (**Additional file 1**).

Discussion

The non-endothelial tdTomato expression patterns observed in this study are likely due to differentiation events traced from endothelial cells. This is supported by previous work that examined the expression pattern of the *VEcad-CreER*^{T2} mouse line used in this study (Monvoisin et al., 2006). Monvoisin et al., found that reporter gene expression by these mice is confined to endothelial cells following a 5-day intraperitoneal injection regimen of 4-hydroxy-tamoxifen (4-OHT) when examined 7 days post-treatment. In addition, inspection of hematopoietic bone marrow cells revealed

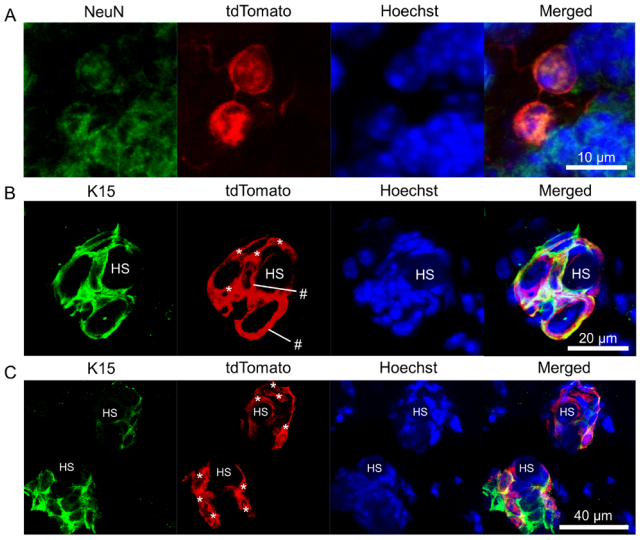

Figure 3 Cerebellar granule neurons and hair follicle stem cells express vascular endothelial-cadherin fate mapping reporter.
Representative confocal microscopy images from adult *VEcad-CreER^{T2}/Rosa-flox-STOP-tdTomato* transgenic mouse cerebellum (A) and skin (B, C) at three months following the start of tamoxifen treatment. Immunohistochemical labeling for (A) NeuN (green) or (B, C) K15 (green) with tdTomato (red) and nucleus (Hoechst; blue) are shown at two magnifications to demonstrate the rare occurrence of K15-tdTomato colocalization. Images captured using a Zeiss Laser Scanning Confocal Microscope Meta 510 system. Orthogonal projections provided in the supplementary data indicate cells exhibiting (#) red/green colocalization. Asterisks (*) signify cells without co-localization, hair shafts (HS) are also shown.

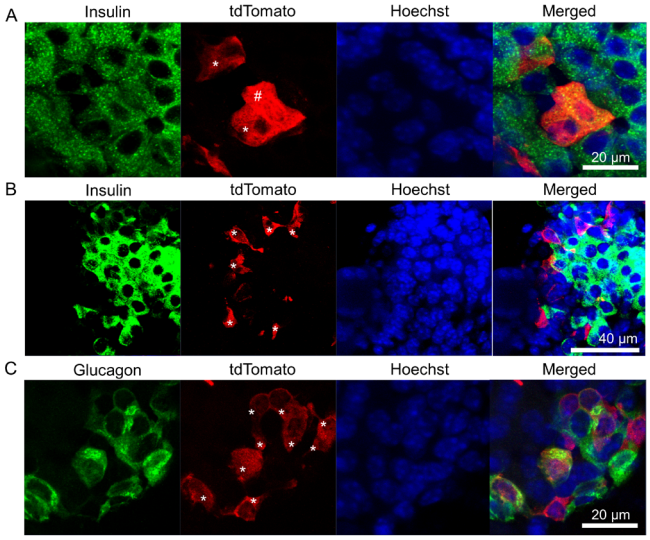

Figure 5 Vascular endothelial-cadherin fate mapping labels pancreatic β-cells.
Immunohistochemistry was performed for pancreatic insulin (A, B) and tdTomato reporter expression at three months post-tamoxifen treatment in adult *VEcad-CreER^{T2}/Rosa-flox-STOP-tdTomato* transgenic mice. Representative images were obtained by confocal microscopy for insulin (A, B; green), glucagon (C; green), tdTomato (red) and the nucleus (Hoechst; blue). Two magnifications of separate fields are shown to demonstrate the rare instances of Insulin-tdTomato colocalization. A Zeiss Laser Scanning Confocal Microscope Meta 510 system was used to capture and analyze the images shown. Confocal orthogonal projections presented in the supplemental data section were utilized to confirm cells with (#) or without (*) green/red co-localization.

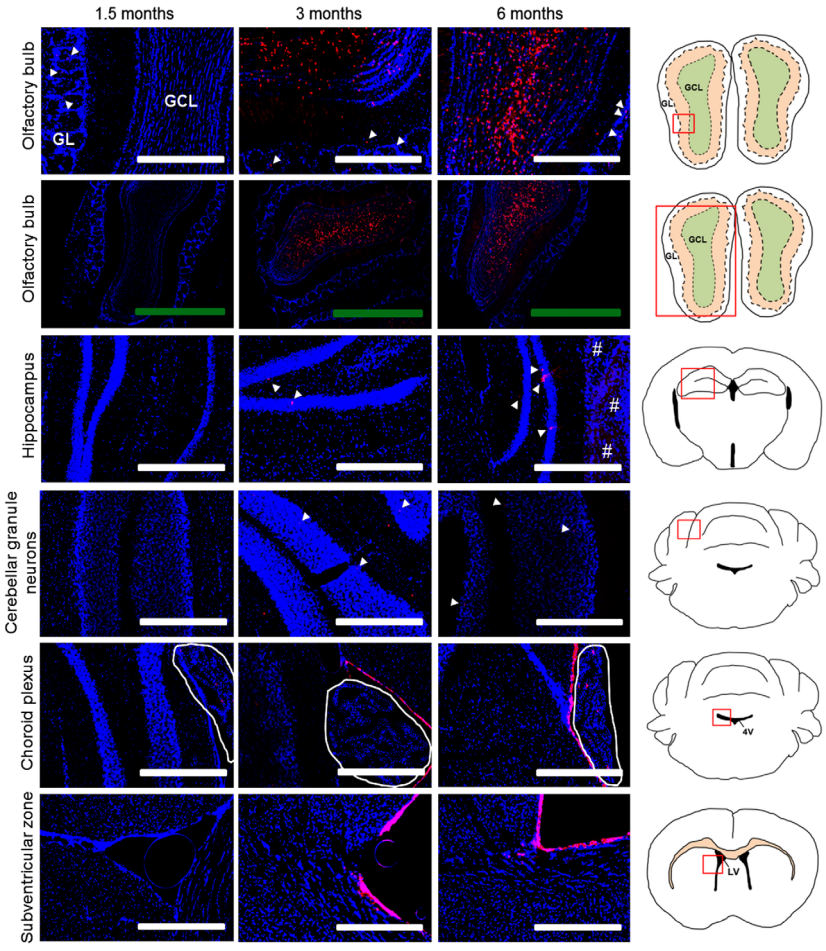

Figure 6 Nestin cell fate mapping in the central nervous system.
Transgenic *Nes-CreER^{T2}/Rosa-flox-STOP-tdTomato* mice at 4–5 months of age were fed tamoxifen-laden chow for 1.5 months and then sacrificed at the times shown post treatment initiation. Channel merged images were then acquired from fixed and Hoechst stained tissues. Nuclei are labeled by Hoechst (blue) and cell lineage tracing is indicated by tdTomato (red). Images shown were obtained from the regions indicated by the red box in the associated diagram to the right where the granule cell layer (GCL), glomerular layer (GL), lateral ventricle (LV) and fourth ventricle (4V) are shown. Arrowheads highlight labeled cells and cellular appendages; # indicates autofluorescence from wrinkled tissue region (white scale bars: 400 µm; green scale bars: 1000 µm).

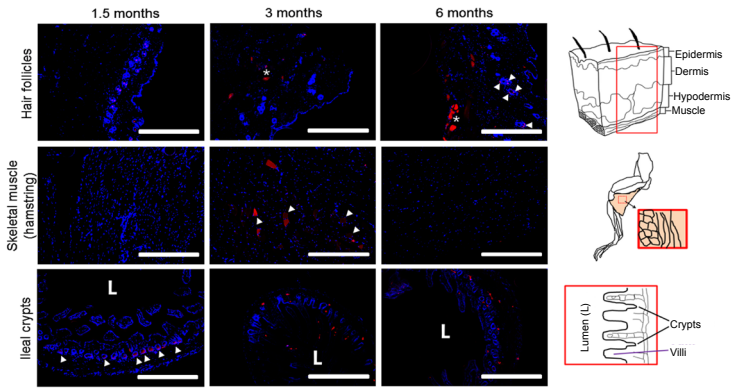

Figure 7 Nestin cell fate mapping in the periphery.
Transgenic *Nes-CreER^{T2}/Rosa-flox-STOP-tdTomato* mice at 4–5 months were fed tamoxifen-laden chow and tissue harvested at the indicated times following treatment initiation. The representative merged channel images were acquired from tissues that were fixed and Hoechst labeled. Cell lineage tracing is evidenced by tdTomato (red) and nuclei are indicated by Hoechst (blue) labeling. Note in hair follicles at 1.5 months after tamoxifen addition, the observed fluorescent signal is only found in hair shafts (no labeled cells). Labeled hair follicle cells observed at 6 months post-tamoxifen were confirmed K15-negative. Red boxes displayed in diagrams on the right indicate region shown in the associated micrographs. Asterisk (*) indicates tdTomato$^+$ muscle fibers underlying skin. Arrowheads highlight labeled cells and the ileal lumen (L) is indicated [white scale bar: 400 μm].

that *VEcad-CreER^{T2}* mice exhibited very few reporter positive cells (0.3%) compared to negative control mice (0.2%) suggesting only a negligible contribution from these sources. This group also assessed skeletal muscle in adult mice (6–8 weeks of age) following 3-day tamoxifen injection at 2 days, 1 week and 6 weeks post-injection. No positive skeletal myocyte reporter expression, only endothelial cells (by morphology), was noted for any time point. This is consistent with our finding of tdTomato+ve skeletal muscle first appearing at 3 months post-treatment. It is important to note that the reporter used by Monvoisin and colleagues to examine *VEcad-CreER^{T2}* mouse line expression utilized a β-galactosidase cassette (activated by CRE activity) residing in the ROSA26 locus and driven by native *ROSA26* elements (Soriano, 1999). Our study utilizes a flox-STOP-tdTomato reporter also residing in the *ROSA26* locus (Madisen et al., 2010). However, this reporter is driven by a CAG promoter that could exhibit differing expression (cell type, intensity and silencing) properties. We observe endothelial cell expression robustly in some tissues while it is markedly reduced in others. This could be due to properties conveyed by the CAG promoter and a possibility that not all endothelial cells exhibit the same expression profile in all tissues. Given the strong endothelial cell fidelity reported by Monvoisin et al. and numerous studies of VE-cadherin immunohistochemistry, the *VEcad-CreER^{T2}* cassette portion of this dual transgenic system appears to be functioning as intended.

The robust labeling of large numbers of cerebellar granule neurons by VE-cadherin tracing was a notable finding. Unlike other regions of the brain, development of the cerebellum begins postnatally, which may represent an alternative development strategy for CGNs. It has been shown that despite elimination of canonical CGN precursors in the early postnatal mouse brain by irradiation and genetic approaches, CGNs are nevertheless generated at high levels (Wojcinski et al., 2017). Ponti et al. (2008) reported that cells previously classified as astroglia and interneuron progenitors are in fact distinct from neonatal canonical CGN progenitors and that in peripubertal rabbits they give rise to large numbers of adult-produced CGNs. A separate group of researchers has also presented evidence indicating that a Nestin-expressing progenitor pool is reprogrammed to contribute to CGN repopulation following acute depletion in postnatal mice (Wojcinski et al., 2017). Interestingly, we also observed Nestin$^+$ progenitors tracing to CGNs. Our study suggests that only a very small number of CGNs are regenerated (absent of injury) from a Nestin-expressing progenitor in adult mice. VE-cadherin$^+$ progenitor cells contribute to the vast majority of labeled CGNs, indicating at least two distinct pools of progenitor cells (Nestin$^+$ and VE-cadherin$^+$) for the homeostasis of adult mouse cerebellum. These findings suggest an opportunity to deliver gene therapy intravenously for direct effects on CGN physiology.

Ependymal cells have been described as a source of CNS progenitor cells in the adult brain (Johansson et al., 1999) in addition to performing other important homeostatic functions such as cerebrospinal fluid production (Becht, 1920; Bruni et al., 1985). Here we report that the ependymal layer is sparsely labeled by VE-cadherin tracing throughout ventricular surfaces 3 months post-TAM (and including the choroid plexus just ventral to the cerebellum). Ependymal labeling was only visible in the choroid plexus adjacent to the cerebellum in the 1.5- and 6-month cohorts. We also observed intense Nestin tracing for the ubiquitous ventricle-lining ependymal layer throughout the adult mouse brain. These results suggest the possibility of a Nestin$^+$/VE-cadherin$^+$ choroid plexus progenitor in adult mice, which is consistent with an endothelial subtype.

This study also revealed VE-cadherin tracing to hair follicle cells. Examination by confocal microscopy revealed that a very small proportion of these cells were positive for a hair follicle stem cell marker (K15). This is a surprising finding, given that hair follicle stem cells are believed to be of mesenchymal origin. As such, K15$^+$ stem cells would not be expected to be derived from a progenitor that expresses an endothelial marker. The highest level of labeling was observed 1.5 months post-TAM where most hair follicles had at least one positive cell per section; significantly reduced labeling was observed at 3 months and labeling was reduced to undetectable levels at 6 months. This implies a rapid turnover rate consistent with hair growth in mice. Unlike VE-cadherin, Nestin did not trace to hair follicle stem cells. We did, however, observe an enrichment of Nestin-traced hair follicle-associated capillaries.

Inspection of skeletal muscle from hamstring showed VE-cadherin tracing at 1.5 months post-TAM treatment

followed by a peak in tdTomato$^+$ muscle fiber number at 3 months. No strongly positive myocytes were observed by 6 months and only faintly labeled fibers remained. This suggests that the signal resulting from the fusion of VE-cadherin-traced progenitors with myocyte cytosol had been diluted out through fusion with non-labeled progenitors after the 3 month post-TAM time point. We also observed Nestin tracing in hamstring at 3 months post-TAM (no labeling in the 1.5- or 6-month cohorts). Additionally, we found VE-cadherin and Nestin tracing to muscle underlying subcutaneous dorsal pelt. This indicates the possible existence of a Nestin$^+$ and VE-cadherin$^+$ skeletal muscle progenitor in adult mice. Previous investigations have reported the existence of skeletal muscle satellite cells in adult animals termed myoendothelial cells that express endothelial cell markers including VE-cadherin (Zheng et al., 2007). Whether these cells are of endothelial origin remains to be determined. Supporting the notion of endothelial-skeletal muscle transdifferentiation are reports of extravascular expression following intravenous delivery of transgenes. A group reported that intravenous delivery of adeno-associated virus (AAV9) containing CRISPR/CAS9 editing constructs, carried out in a canine model of Duchenne muscular dystrophy (Amoasii et al., 2018), resulted in successful editing of a mutant dystrophin gene in skeletal muscle. Interestingly, this group found an extremely high percentage of successfully edited/transduced skeletal myocytes at 2 months post-systemic AAV injection, even far surpassing what was observed in this study. Taken together, these findings imply that intravenous delivery of gene therapy could be undertaken to correct a defined mutation or provide a trophic factor to improve outcomes for skeletal muscle disease.

Investigation of VE-cadherin cell lineage tracing within the pancreas uncovered tdTomato labeling of islets. All islets examined at 1.5 months post-TAM contained tdTomato$^+$ cells and 83% of islets at 3 months post-TAM displayed labeling. No labeling was evident at 6 months, suggesting complete turnover of labeled cells by that time. Confocal assessment confirmed that a small proportion (3%) of tdTomato$^+$ islet cells were insulin-producing β cells. No tdTomato-expressing cells were found to be glucagon$^+$ α-cells. The presence of VE-cadherin-traced β cells suggests the possible existence of a β cell precursor cell in adult mice with endothelial origins. The evident decrease in tdTomato$^+$ islet cells over time provides support for the existence of regenerative mechanisms of β cells in adult mice, which is currently a subject of controversy (Yu et al., 2016). The existence of a natural endothelial-derived β cell progenitor could offer new intravenous therapy options for prolonged treatment of diabetes. In addition, this knowledge could inform strategies to stimulate β cell regeneration *in vivo*.

Exocrine pancreatic acini were also found to contain tdTomato-labeled cells following VE-cadherin tracing. Only a few acini lobes per section exhibited the fluorescent marker, though when present, positive cells were grouped in close proximity. The highest abundance of labeled acini was found 1.5 months post-TAM, which decreased markedly 3 months after treatment. The 6-month group showed only rare and individual tdTomato$^+$ acinar cells. This labeling pattern suggests the existence of an endothelial-derived progenitor and that near-complete regeneration of acini cells occurred over this 6-month period.

Renal tissue was also found to exhibit VE-cadherin tracing. Specifically, cells comprising the convoluted tubules within the renal cortex had pronounced labeling at 1.5 months post-TAM, with a gradual loss observed at 3 months and only a very faint signal detected at 6 months. The progenitor source for adult proximal convoluted tubule cells is still highly debated and our finding adds to a substantial body of evidence regarding extra-renal and atypical sources (Poulsom et al., 2001; Gupta et al., 2002; Sugimoto et al., 2006; Castrop, 2019). The observed fluorescent signal in this study likely does not arise from filtrate since the tissues were thoroughly flushed during multiple washes following sectioning onto slides. In addition, tdTomato labeling is completely absent from the renal medulla, excluding fluorescence contributed directly by filtrate cells in the loop of Henle or medullar collecting tubules. However, it cannot be ruled out that label-positive proximal convoluted tubule cells obtained tdTomato from early filtrate via their native protein-recovery mechanisms and thereby obtained cytosolic fluorescence independent of a transdifferentiation event. An alternative interpretation of this result could be that cell fusion events of proximal convoluted tubule cells with other tdTomato$^+$ cells decreased and that contributed cytoplasm was gradually turned over (similar to myocytes). Another possibility is that the weak signal at 6 months is due to activation of CRE by tamoxifen that has persisted. Further studies are needed to explore these possibilities as the prospect for renewal of these important cell types could be useful in the development of therapeutic strategies for the treatment of kidney disease.

Our assessment of the digestive tract revealed VE-cadherin cell lineage tracing of duodenal and ileal gland crypts. Labeling was confined to the base of the intestinal crypts and was robust at 1.5 months but disappeared 3 months after TAM treatment began. This suggests a rapid turnover of these cells, which is consistent with that of cells found within a highly proliferative epithelial tissue. A weaker fluorescent signal was observed for more mature cells emanating from the crypts that form the intestinal villi. Interestingly, we did not observe any tdTomato labeling within colonic crypts, which suggests a different etiology in adult mice. We also found that Nestin traced to Ileal crypts at 1.5 months post-TAM (and disappeared by 3 months) but did not trace to the duodenum suggesting divergent origins for these adult tissues.

Conclusion

There is evidence of tissue homeostasis by actively dividing stem cells and one or more pools of quiescent stem cells working in concert to maintain cell replacement needs (Li and Clevers, 2010; Blanpain and Fuchs, 2014). In such cases, it is possible that the selector of the donating quiescent progenitor is the tissue environment rather than the cell type

classification of the progenitor itself. For example, a growing body of evidence indicates that some quiescent brain regions possess the ability to foster the differentiation of transplanted progenitor cells from varied sources into functional neurons (Lindvall et al., 1989; Volkman and Offen, 2017). Moreover, experimental ablation of one type of progenitor can cause restoration by another type (Rompolas et al., 2013; Blanpain and Fuchs, 2014). If indeed this form of plasticity occurs broadly in adult mammals, endothelial cells would represent the most readily available cell type for "recruitment" as a progenitor across tissues. Evidence presented in this study supports the notion of an endothelial population that transdifferentiates into other embryonically distinct cell types and which is also a substantial contributor to adult mammalian tissue homeostasis. Confirmation of such a finding would offer new insights into the pathology of human disease and present potential therapeutic avenues.

Limitations of the CreERT2/Rosa-floxed-STOP-tdTomato system

a) Cell fusion events cannot be completely ruled out. However, Hoechst labeling of nuclei did not reveal any multinucleated cells (with the exception of myocytes) by conventional or confocal microscopy. In addition, previous studies involving bone marrow-derived stem cell transplantation (Alvarez-Dolado et al., 2003) did not reveal cell fusion events for any of the tdTomato^{+} cells observed in this study, indicating that tdTomato-expressing cells are likely not derived from fusion events with hematopoietic cells (e.g., B-cells).

b) The genomic location (*Rosa26*) of the reporter cassette, in concert with the exogenous promoter employed (CAG promoter-driven-tdTomato), dictates the cell-type expression pattern of tdTomato following the initial activation from flox-STOP removal by CreER^{T2}. Therefore, genomic editing by activated CreER^{T2} may have occurred in a given cell without the production of a fluorescent signal if the *Rosa26* locus or CAG promoter is silenced by that cell type.

c) CRE activity can result in two outcomes. Correct editing creates a tdTomato sequence with the removal of a stop-codon-containing cassette and the subsequent expression of a functional fluorescent reporter. However, CRE activity can also result in translocation of cut DNA fragments to other locations in the genome or other rearrangements that do not produce a functional reporter. In these instances, cell lineage tracing mechanisms would be activated but not observed.

d) Promoter silencing is a reported cellular response to numerous constitutive promoter systems (e.g., CMV, CAG) (Choi et al., 2005; Xia et al., 2007; Herbst et al., 2012). Reporter gene silencing could also confound the disappearance of the tdTomato signal at later time points. Other approaches would be necessary to determine if a loss in signal is due to cell turnover or CAG promoter silencing.

e) The observation of fewer reported tracing events could be the result of cell death. Double-stranded cuts directed by CRE in target cells initiate DNA repair systems. If repairs are not made correctly or in a timely fashion, cells are susceptible to apoptosis. In addition, cell death could be directed by the immune system against tdTomato-derived peptides presented in MHC class I complexes. However, this prospect is unlikely, given that tdTomato is observed in some tissues in both VE-cadherin and Nestin mouse lines at 6 months post-TAM.

f) Contributions by extracellular vesicles emitted from tdTomato-expressing cells cannot be determined in this system. It is possible that extracellular vesicles containing tdTomato are released by edited/labeled cells and accumulated in target cells, thereby leading to fluorescence in the target cell that is not associated with a transdifferentiation event. This is an inherent limitation of the Rosa-floxed-STOP-tdTomato system.

Acknowledgments: *We would like to express our sincere thanks to Dr. Luisa Iruela-Arispe (University of California, Los Angeles, USA) for gifting us VEcad-CreERT2 transgenic mice.*
Author contributions: *ASA and BEM designed and conducted experiments as well as interpreted results. BEM wrote the original manuscript draft while ASA and BEM reviewed and edited this document.*
Conflicts of interest: *The authors declare no conflict of interests regarding the work described in this report.*
Financial support: *This study was supported by the National Institutes Health (grant Nos. 5P20GM109095 and P20GM103408) and Boise State University.*
Institutional review board statement: *The animal experiments were approved by the Boise State University Institute Animal Care and Use Committee (approval No. 006-AC15-018) on October 31, 2018.*

Data sharing statement: *Datasets analyzed during the current study are available from the corresponding author on reasonable request.*
Plagiarism check: *Checked twice by iThenticate.*
Peer review: *Externally peer reviewed.*

Additional files:

Additional file 1: *VE-cadherin and Nestin cell fate mapping image repository.*
Additional Figure 1: *Prototypical arterial endothelial cell expression of tdTomato following VE-cadherin cell lineage tracing in renal tissue.*
Additional Figure 2: *Confocal microscopy orthogonal analysis of VE-cadherin-traced cerebellar granule neurons and hair follicle cells presented in Figure 3.*
Additional Figure 3: *Examination of skeletal myocytes following VE-cadherin cell lineage tracing high resolution confocal image.*
Additional Figure 4: *VE-cadherin-traced cerebellar granule neurons confocal microscopy high resolution tiled image.*
Additional Figure 5: *Confocal microscopy orthogonal analysis of VE-cadherin-traced pancreatic islet cells presented in Figure 5.*
Additional Figure 6: *VE-cadherin cell lineage tracing high-resolution confocal image of pancreatic acini.*

References

Albright JE, Stojkovska I, Rahman AA, Brown CJ, Morrison BE (2016) Nestin-positive/SOX2-negative cells mediate adult neurogenesis of nigral dopaminergic neurons in mice. Neurosci Lett 615:50-54.

Altman J (1969) Autoradiographic and histological studies of postnatal neurogenesis. IV. Cell proliferation and migration in the anterior forebrain, with special reference to persisting neurogenesis in the olfactory bulb. J Comp Neurol 137:433-457.

Altman J, Das GD (1965) Autoradiographic and histological evidence of postnatal hippocampal neurogenesis in rats. J Comp Neurol 124:319-335.

Alvarez-Dolado M, Pardal R, Garcia-Verdugo JM, Fike JR, Lee HO, Pfeffer K, Lois C, Morrison SJ, Alvarez-Buylla A (2003) Fusion of bone-marrow-derived cells with Purkinje neurons, cardiomyocytes and hepatocytes. Nature 425:968-973.

Amoasii L, Hildyard JCW, Li H, Sanchez-Ortiz E, Mireault A, Caballero D, Harron R, Stathopoulou T-R, Massey C, Shelton JM, Bassel-Duby R, Piercy RJ, Olson EN (2018) Gene editing restores dystrophin expression in a canine model of Duchenne muscular dystrophy. Science 362:86-91.

Battiste J, Helms AW, Kim EJ, Savage TK, Lagace DC, Mandyam CD, Eisch AJ, Miyoshi G, Johnson JE (2007) Ascl1 defines sequentially generated lineage-restricted neuronal and oligodendrocyte precursor cells in the spinal cord. Development 134:285-293.

Bayer SA, Yackel JW, Puri PS (1982) Neurons in the rat dentate gyrus granular layer substantially increase during juvenile and adult life. Science 216:890-892.

Becht FC (1920) Studies on the cerebrosp inal fluid. American Journal of Physiology-Legacy Content 51:1-125.

Bernanke DH, Markwald RR (1982) Migratory behavior of cardiac cushion tissue cells in a collagen-lattice culture system. Dev Biol 91:235-245.

Bifari F, Decimo I, Pino A, Llorens-Bobadilla E, Zhao S, Lange C, Panuccio G, Boeckx B, Thienpont B, Vinckier S, Wyns S, Bouche A, Lambrechts D, Giugliano M, Dewerchin M, Martin-Villalba A, Carmeliet P (2017) Neurogenic radial glia-like cells in meninges migrate and differentiate into functionally integrated neurons in the neonatal cortex. Cell Stem Cell 20:360-373.

Blanpain C, Fuchs E (2014) Stem cell plasticity. Plasticity of epithelial stem cells in tissue regeneration. Science 344:1242281.

Bruni JE, Del Bigio MR, Clattenburg RE (1985) Ependyma: normal and pathological. A review of the literature. Brain Res 356:1-19.

Camenisch TD, Molin DGM, Person A, Runyan RB, Gittenberger-de Groot AC, McDonald JA, Klewer SE (2002) Temporal and distinct TGFbeta ligand requirements during mouse and avian endocardial cushion morphogenesis. Dev Biol 248:170-181.

Castrop H (2019) The role of renal interstitial cells in proximal tubular regeneration. Nephron 141:265-272.

Chen PY, Qin L, Baeyens N, Li G, Afolabi T, Budatha M, Tellides G, Schwartz MA, Simons M (2015) Endothelial-to-mesenchymal transition drives atherosclerosis progression. J Clin Invest 125:4514-4528.

Choi KH, Basma H, Singh J, Cheng P-W (2005) Activation of CMV promoter-controlled glycosyltransferase and beta-galactosidase glycogenes by butyrate, tricostatin A, and 5-aza-2′-deoxycytidine. Glycoconj J 22:63-69.

de Lange FJ, Moorman AFM, Anderson RH, Männer J, Soufan AT, de Gier-de Vries C, Schneider MD, Webb S, van den Hoff MJB, Christoffels VM (2004) Lineage and morphogenetic analysis of the cardiac valves. Circ Res 95:645-654.

Ding L, Morrison SJ (2013) Haematopoietic stem cells and early lymphoid progenitors occupy distinct bone marrow niches. Nature 495:231-235.

Donato AJ, Morgan RG, Walker AE, Lesniewski LA (2015) Cellular and Molecular Biology of Aging Endothelial Cells. J Mol Cell Cardiol 89(Pt B):122-135.

Dusart P, Fagerberg L, Perisic L, Civelek M, Struck E, Hedin U, Uhlén M, Trégouët D-A, Renné T, Odeberg J, Butler LM (2018) A systems-approach reveals human nestin is an endothelial-enriched, angiogenesis-independent intermediate filament protein. Sci Rep 8:14668.

Eisenberg LM, Markwald RR (1995) Molecular regulation of atrioventricular valvuloseptal morphogenesis. Circ Res 77:1-6.

Gupta S, Verfaillie C, Chmielewski D, Kim Y, Rosenberg ME (2002) A role for extrarenal cells in the regeneration following acute renal failure. Kidney Int 62:1285-1290.

Heimark RL, Degner M, Schwartz SM (1990) Identification of a Ca2(+)-dependent cell-cell adhesion molecule in endothelial cells. J Cell Biol 110:1745-1756.

Herbst F, Ball CR, Tuorto F, Nowrouzi A, Wang W, Zavidij O, Dieter SM, Fessler S, van der Hoeven F, Kloz U, Lyko F, Schmidt M, von Kalle C, Glimm H (2012) Extensive methylation of promoter sequences silences lentiviral transgene expression during stem cell differentiation in vivo. Mol Ther 20:1014-1021.

Hussaini SMQ, Jun H, Cho CH, Kim HJ, Kim WR, Jang MH (2013) Heat-induced antigen retrieval: an effective method to detect and identify progenitor cell types during adult hippocampal neurogenesis. J Vis Exp doi: 10.3791/50769.

Itkin T, Gur-Cohen S, Spencer JA, Schajnovitz A, Ramasamy SK, Kusumbe AP, Ledergor G, Jung Y, Milo I, Poulos MG, Kalinkovich A, Ludin A, Kollet O, Shakhar G, Butler JM, Rafii S, Adams RH, Scadden DT, Lin CP, Lapidot T (2016) Distinct bone marrow blood vessels differentially regulate haematopoiesis. Nature 532:323-328.

Johansson CB, Momma S, Clarke DL, Risling M, Lendahl U, Frisén J (1999) Identification of a neural stem cell in the adult mammalian central nervous system. Cell 96:25-34.

Kretzschmar K, Watt FM (2012) Lineage tracing. Cell 148:33-45.

Li L, Clevers H (2010) Coexistence of quiescent and active adult stem cells in mammals. Science 327:542-545.

Li Y, Lui KO, Zhou B (2018) Reassessing endothelial-to-mesenchymal transition in cardiovascular diseases. Nat Rev Cardiol 15:445-456.

Lindvall O, Rehncrona S, Brundin P, Gustavii B, Astedt B, Widner H, Lindholm T, Björklund A, Leenders KL, Rothwell JC, Frackowiak R, Marsden D, Johnels B, Steg G, Freedman R, Hoffer BJ, Seiger A, Bygdeman M, Strömberg I, Olson L (1989) Human fetal dopamine neurons grafted into the striatum in two patients with severe Parkinson's disease. A detailed account of methodology and a 6-month follow-up. Arch Neurol 46:615-631.

Madisen L, Zwingman TA, Sunkin SM, Oh SW, Zariwala HA, Gu H, Ng LL, Palmiter RD, Hawrylycz MJ, Jones AR, Lein ES, Zeng H (2010) A robust and high-throughput Cre reporting and characterization system for the whole mouse brain. Nat Neurosci 13:133-140.

Menezes JR, Smith CM, Nelson KC, Luskin MB (1995) The division of neuronal progenitor cells during migration in the neonatal mammalian forebrain. Mol Cell Neurosci 6:496-508.

Merrell AJ, Stanger BZ (2016) Adult cell plasticity in vivo: trans-differentiation is back in style. Nat Rev Mol Cell Biol 17:413-425.

Michalopoulos GK, Barua L, Bowen WC (2005) Transdifferentiation of rat hepatocytes into biliary cells after bile duct ligation and toxic biliary injury. Hepatology 41:535-544.

Mjaatvedt CH, Lepera RC, Markwald RR (1987) Myocardial specificity for initiating endothelial-mesenchymal cell transition in embryonic chick heart correlates with a particulate distribution of fibronectin. Dev Biol 119:59-67.

Mokrý J, Ehrmann J, Karbanová J, Cízková D, Soukup T, Suchánek J, Filip S, Kolár Z (2008) Expression of intermediate filament nestin in blood vessels of neural and non-neural tissues. Acta Medica (Hradec Kralove) 51:173-179.

Monvoisin A, Alva JA, Hofmann JJ, Zovein AC, Lane TF, Iruela-Arispe ML (2006) VE-cadherin-CreERT2 transgenic mouse: a model for inducible recombination in the endothelium. Dev Dyn 235:3413-3422.

Moonen JR, Lee ES, Schmidt M, Maleszewska M, Koerts JA, Brouwer LA, van Kooten TG, van Luyn MJ, Zeebregts CJ, Krenning G, Harmsen MC (2015) Endothelial-to-mesenchymal transition contributes to fibro-proliferative vascular disease and is modulated by fluid shear stress. Cardiovasc Res 108:377-386.

Oh M, Nör JE (2015) The perivascular niche and self-renewal of stem cells. Front Physiol 6:367.

Palmer TD, Ray J, Gage FH (1995) FGF-2-responsive neuronal progenitors reside in proliferative and quiescent regions of the adult rodent brain. Mol Cell Neurosci 6:474-486.

Ponti G, Peretto P, Bonfanti L (2008) Genesis of neuronal and glial progenitors in the cerebellar cortex of peripuberal and adult rabbits. PLoS One 3:e2366.

Poulsom R, Forbes SJ, Hodivala-Dilke K, Ryan E, Wyles S, Navaratnarasah S, Jeffery R, Hunt T, Alison M, Cook T, Pusey C, Wright NA (2001) Bone marrow contributes to renal parenchymal turnover and regeneration. J Pathol 195:229-235.

Rahman AA, Lai NK, Albright JE, Urquhart PE, Webb AR, Morrison BE (2017) Nigral dopaminergic neuron replenishment in adult mice through VE-cadherin-expressing neural progenitor cells. Neural Regen Res 12:1865-1869.

Rompolas P, Mesa KR, Greco V (2013) Spatial organization within a niche as a determinant of stem-cell fate. Nature 502:513-518.

Soriano P (1999) Generalized lacZ expression with the ROSA26 Cre reporter strain. Nat Genet 21:70-71.

Sugimoto H, Mundel TM, Sund M, Xie L, Cosgrove D, Kalluri R (2006) Bone-marrow-derived stem cells repair basement membrane collagen defects and reverse genetic kidney disease. Proc Natl Acad Sci U S A 103:7321-7326.

Suzuki S, Namiki J, Shibata S, Mastuzaki Y, Okano H (2010) The neural stem/progenitor cell marker nestin is expressed in proliferative endothelial cells, but not in mature vasculature. J Histochem Cytochem 58:721-730.

Tamplin OJ, Durand EM, Carr LA, Childs SJ, Hagedorn EJ, Li P, Yzaguirre AD, Speck NA, Zon LI (2015) Hematopoietic stem cell arrival triggers dynamic remodeling of the perivascular niche. Cell 160:241-252.

Tang Z, Wang A, Yuan F, Yan Z, Liu B, Chu JS, Helms JA, Li S (2012) Differentiation of multipotent vascular stem cells contributes to vascular diseases. Nat Commun 3:875.

Tarlow BD, Pelz C, Naugler WE, Wakefield L, Wilson EM, Finegold MJ, Grompe M (2014) Bipotential adult liver progenitors are derived from chronically injured mature hepatocytes. Cell Stem Cell 15:605-618.

Volkman R, Offen D (2017) Concise review: mesenchymal stem cells in neurodegenerative diseases. Stem Cells 35:1867-1880.

Wojcinski A, Lawton AK, Bayin NS, Lao Z, Stephen DN, Joyner AL (2017) Cerebellar granule cell replenishment postinjury by adaptive reprogramming of Nestin+ progenitors. Nat Neurosci 20:1361-1370.

Wurmser AE, Nakashima K, Summers RG, Toni N, D'Amour KA, Lie DC, Gage FH (2004) Cell fusion-independent differentiation of neural stem cells to the endothelial lineage. Nature 430:350-356.

Xia X, Zhang Y, Zieth CR, Zhang SC (2007) Transgenes delivered by lentiviral vector are suppressed in human embryonic stem cells in a promoter-dependent manner. Stem Cells and Dev 16:167-176.

Yu K, Fischbach S, Xiao X (2016) Beta cell regeneration in adult mice: controversy over the involvement of stem cells. Curr Stem Cell Res Ther 11:542-546.

Zerlin M, Levison SW, Goldman JE (1995) Early patterns of migration, morphogenesis, and intermediate filament expression of subventricular zone cells in the postnatal rat forebrain. J Neurosci 15:7238-7249.

Zheng B, Cao B, Crisan M, Sun B, Li G, Logar A, Yap S, Pollett JB, Drowley L, Cassino T, Gharaibeh B, Deasy BM, Huard J, Peault B (2007) Prospective identification of myogenic endothelial cells in human skeletal muscle. Nat Biotechnol 25:1025-1034.

C-Editors: Zhao M, Li CH; T-Editor: Jia Y

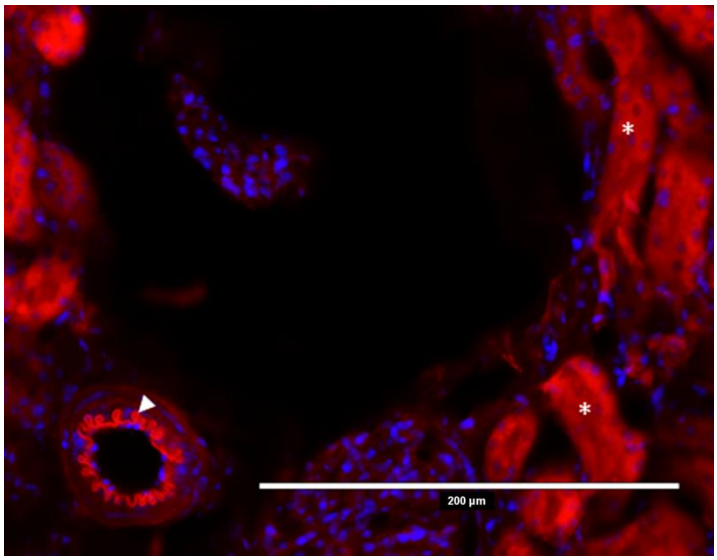

Additional Figure 1 Prototypical arterial endothelial cell expression of tdTomato following VE-cadherin cell lineage tracing in renal tissue.

Renal tissue was harvested from *VEcad-CreER^{T2}/Rosa-flox-STOP-tdTomato* transgenic mice 1.5 months post-tamoxifen treatment initiation. Tissue samples were fixed, cryosectioned (15 µm) onto slides, stained with Hoechst dye (nuclear label) and then mounted with coverslips. The displayed image was captured by an EVOS M7000 conventional fluorescence microscopy system. The merged image shows tdTomato (red) and Hoechst (blue) channels. Arrowhead indicates tdTomato+ endothelial cells of the internal elastic lamina of a renal glomerulus arteriole. Asterisks (*) show tdTomato+ convoluted tubules also present in this micrograph.

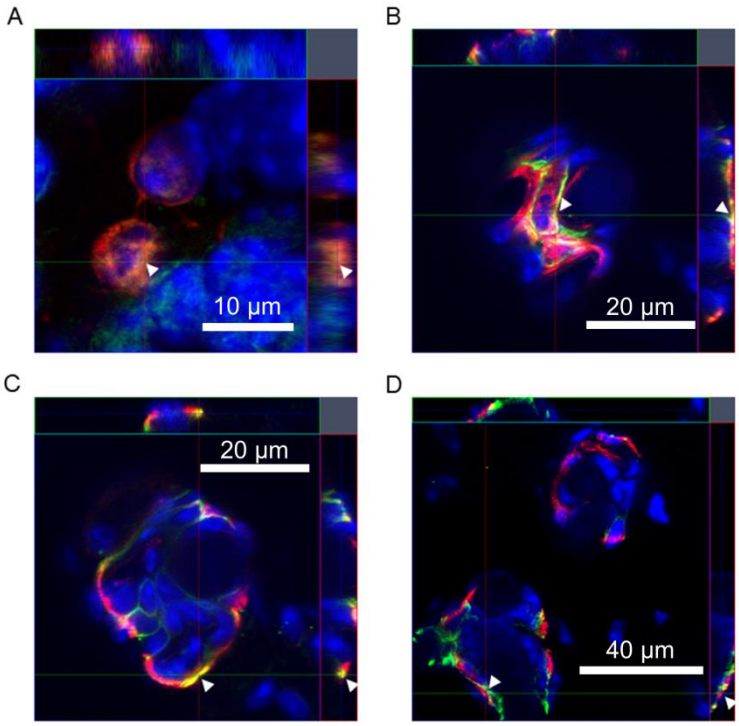

Additional Figure 2 Confocal microscopy orthogonal analysis of VE-cadherin-traced cerebellar granule neurons and hair follicle cells presented in Figure 3.

(A) NeuN (green) /tdTomato (red) co-labeling (arrowheads) by IHC confirmed for cerebellar granule neurons through orthogonal reconstruction from confocal image stacks. **(B, C)** Rare hair follicular cells exhibit K15 (green)/tdTomato (red) co-localization (arrowheads). **(D)** The vast majority of tdTomato hair follicle cells do not exhibit co-labeling with K15 (green) despite often being in very close proximity. Images captured using a Zeiss Laser Scanning Confocal Microscope Meta 510 system.

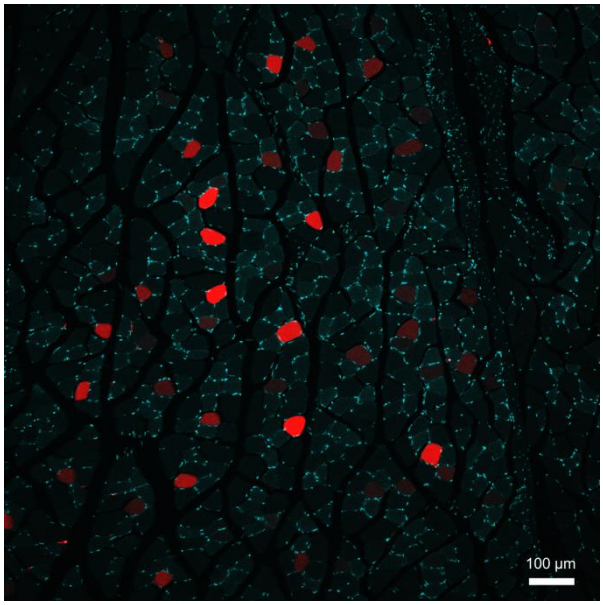

Additional Figure 3 Examination of skeletal myocytes following VE-cadherin cell lineage tracing high resolution confocal image.

Hamstring tissue was harvested from *VEcad-CreER^{T2}/Rosa-flox-STOP-tdTomato* transgenic mice 3 months post-tamoxifen treatment initiation. Fixed samples were sectioned (15 µm) onto slides, labeled with Hoechst dye, mounted with coverslips and imaged using an Olympus FV3000 Laser Scanning Confocal Microscope system. The displayed image was obtained from a series of 10 µm z-stacked planes compressed into a maximum intensity projection image showing tdTomato (red) and Hoechst (blue) channels.

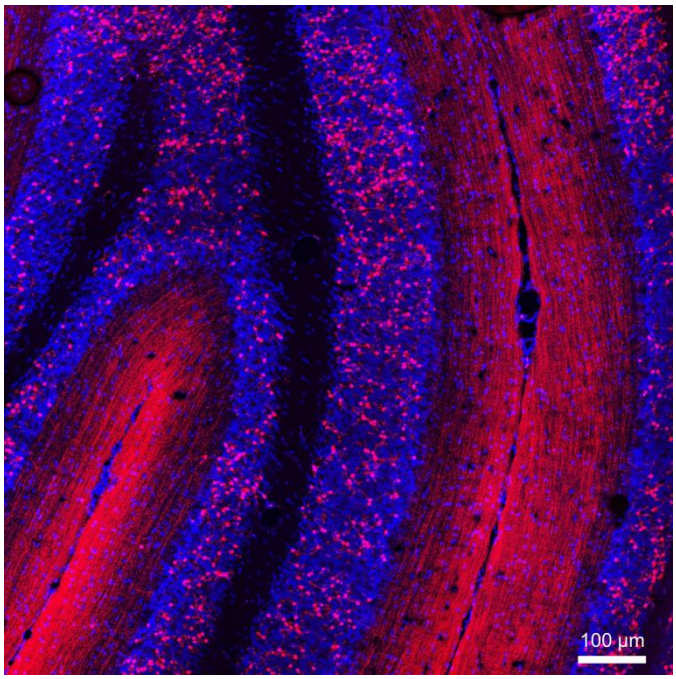

Additional Figure 4 VE-cadherin-traced cerebellar granule neurons confocal microscopy high resolution tiled image.

Tissue was harvested from *VEcad-CreER^{T2}/Rosa-flox-STOP-tdTomato* transgenic mice 3 months post-tamoxifen treatment initiation. The cryosectioned tissue (15 µm) was fixed, labeled with Hoechst dye and mounted with a coverslip. A tiled image was captured for 10 µm z-stacked planes and stitched using a Zeiss 880 Airy Scan system. Hoechst dye (blue) and tdTomato (red) channels are displayed in the maximum intensity projection image shown.

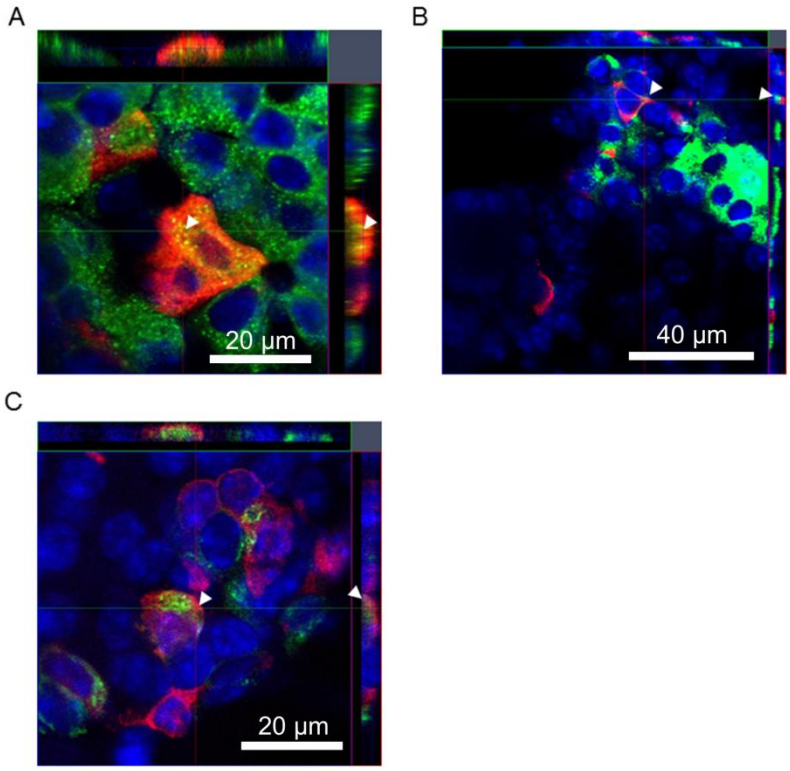

Additional Figure 5 Confocal microscopy orthogonal analysis of VE-cadherin-traced pancreatic islet cells presented in Figure 5.

(A) Immunohistochemistry for insulin/tdTomato-co-labeled cell (arrowhead) assessed by orthogonal reconstruction from confocal stacked images. **(B)** Almost all tdTomato positive islet cells examined are insulin (green)-negative despite very close physical proximity. **(C)** No glucagon (green)/tdTomato co-labeled cells were observed in any pancreatic section examined. Arrowheads indicate a point of assessment. A Zeiss Laser Scanning Confocal Microscope Meta 510 system was used to capture and analyze the images shown.

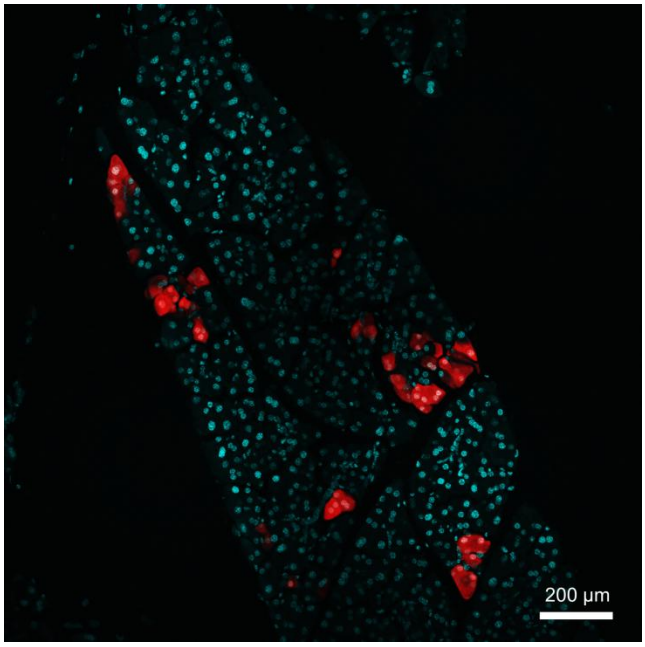

Additional Figure 6 VE-cadherin cell lineage tracing high-resolution confocal image of pancreatic acini.

Pancreatic tissue was harvested from *VEcad-CreER^{T2}/Rosa-flox-STOP-tdTomato* transgenic mice 3 months post-tamoxifen treatment initiation. Tissue samples were fixed, cryosectioned (15 µm) onto slides, stained with Hoechst dye and then mounted with coverslips. The displayed image was captured by an Olympus FV3000 Laser Scanning Confocal Microscope system from 10 µm z-stacked planes and represented as a maximum intensity projection. The merged image shows tdTomato (red) and Hoechst (blue) channels.